

3D simulation of the plasma jet in thermal plasma spraying

Fan Qunbo*, Wang Lu, Wang Fuchi

School of Material Science and Engineering, Beijing Institute of Technology, Beijing 100081, China

Received 20 December 2002; received in revised form 4 May 2004; accepted 19 August 2004

Abstract

In this paper, a continuous medium model and the $k-\varepsilon$ turbulence formulations are employed to predict the plasma velocity, plasma temperature and argon molar concentration fields in three-dimensional (3D) space. Some important 3D information, such as the 3D continuous isothermal lines, isovelocity lines and the 3D appearance of the plasma jet, are described. This is hard to obtain directly using a 2D scheme. The calculated results will be theoretically helpful for further analysis of the temperature history and trajectories of the entrained particles, particle molten status in the plasma jet, and the deposition of the coatings.

© 2004 Elsevier B.V. All rights reserved.

Keywords: 3D simulation; Plasma jet; Thermal plasma spraying

1. Introduction

For a considerable time, particular attention has been paid to the numerical simulation of the plasma jet. The axial and radial temperature and velocity distribution (temperature fields and velocity fields) in the plasma jet affect significantly the particle temperature and its flying behavior, and hence the quality of the coating. Therefore, it is desirable to study the heat transfer and fluid flow of the plasma jet.

Plasma flames for thermal spraying can produce temperatures around 7000–20,000 K far above the melting temperature (and vapor temperature) of any known material. Unfortunately, at the extremely high-temperature levels, the phenomena differ significantly from those occurring at room temperature or extrapolated from room temperature behavior. This makes modeling work much more complex, characterized by its own specific features. Therefore, Eckert and Pfender [1] provided a comprehensive introduction to plasma heat transfer which is of fundamental importance in this area. The early studies, however, were restricted to laminar flow situations and most real plasma reactors represent turbulent characteristics. To solve this problem, a standard or a modified $K-\varepsilon$ turbulence model [2] was employed, which was assumed to be still valid for plasma jets. Up to the present time, the sci-

entific basis of these operations has been concerned with 2D fluid turbulence models [3–5] to avoid a complicated computation.

However, a three-dimensional (3D) geometric configuration has to be taken into account to predict the temperature history of groups of particles (especially multi-group particles of different materials), the dispersion of particles in the jet flow, and the deposition process of the coatings. Dussoubs et al. [6] proposed a 3D model to solve the coupled conservation equations of mass, species, momentum and thermal energy equations for a compressible and turbulent plasma jet. The effect of process variables on the plasma jet flow fields was discussed. However, a more comprehensive study is still necessary. Here, the 3D temperature and velocity fields, and the distribution of species are calculated in finite difference methods by using a commercial computational fluid dynamics package, FLUENT [7]. Some important 3D information, such as the 3D continuous isothermal lines, isovelocity lines, and the 3D appearance of the plasma jet are described. This is hard to obtain directly using a 2D scheme.

2. Mathematical model

In plasma spraying, the plasma gases ionize and dissociate because of the energy of the plasma arc. By re-combination of the atoms and molecules outside the nozzle the received

* Corresponding author. Fax: +86 10 68913951 88.
E-mail address: fanqunbo@bit.edu.cn (F. Qunbo).

Nomenclature

D	mass diffusion coefficient (m ² /s)
f	net production rate of species
\vec{F}_i	external body or surface force acting on species (N)
G	dissipation function (W/m ³)
h	enthalpy (W/m ² K)
\vec{J}	diffusion flux (kg/(m ² s))
K	turbulent kinetic energy (m ² /s ²)
\vec{P}	pressure (Pa)
\vec{q}	rate of quantity of heat fluxing into the control volume (W/m ²)
t	time (s)
\vec{U}	diffusion velocity vector (m/s)
\vec{v}	velocity vector (m/s)
x	velocity component

Greek letters

ε	turbulent energy dissipation rate (m ² /s ³)
μ	dynamic viscosity (kg/(m s))
ρ	density (kg/m ³)
$\vec{\tau}$	stress tensor (N/m ²)
Φ	rate of energy loss by viscous friction (W/m ²)

Subscripts

i	species i
j	in the direction of j
t	turbulence

Turbulence parameters

C_1	1.44
C_2	1.92
C_μ	0.09
σ_k	1.0
σ_ε	1.3

energy is suddenly set free and intensifies the thermal impact of the plasma beam on the substrate. Therefore, the theory of continuous medium and free jet can be applied. The governing equations can be represented by the mass continuity equation, the conservation equation of momentum, the conservation equation of energy and a standard K – ε equation.

The model is based on the following assumptions:

- (1) The plasma is in local thermodynamic equilibrium, i.e. the temperature of the gas atoms, ions and electrons at a point are equal, and therefore can be characterized by a single temperature.
- (2) The plasma gas is a continuous multi-component chemically reacting ideal gas, which is composed of three gases: Ar, H₂ and N₂. At the extremely high-temperature levels, the diatomic molecules H₂ and N₂ dissociations

are nearly complete, i.e. the plasma gas leaving the gun exit is composed of six species: Ar, Ar⁺, H, H⁺, N and N⁺.

- (3) The energy loss by radiation is negligible.
- (4) During a certain period, the plasma jet flow is in a steady-state system.
- (5) There are no chemical reactions in the gas phase.

2.1. Conservation of mass

Based on the assumption that there is no mass added to the continuous plasma gas, the rate of change of the fluid mass in control volume is equal to the overall fluid mass flowing into the volume, which may be expressed as

$$\frac{\partial \rho}{\partial t} = -\nabla \cdot (\rho \vec{v}) \quad (1)$$

where ρ is the local density of the plasma gas, t the time, and \vec{v} the gas velocity vector.

On the other hand, if f_i is defined as the net production rate of species i , i.e.

$$f_i = \frac{\rho_i}{\rho} \quad (2)$$

$$\sum f_i = 1 \quad (3)$$

then the mass flux of species i can be given by the sum of $\rho_i \vec{v}$ plus the diffusion flux $\rho_i \vec{U}_i$:

$$\rho_i \vec{v}_i = \rho_i (\vec{v} + \vec{U}_i) = \rho_i \vec{v} + \rho_i \vec{U}_i \quad (4)$$

where \vec{v}_i and \vec{U}_i are the velocity and diffusion velocity vectors of species i , respectively. According to the law of Fick, the diffusion flux \vec{J}_i can be given by

$$\vec{J}_i = \rho_i \vec{U}_i = -\rho D_i (\nabla f_i) \quad (5)$$

where D_i is the mass diffusion coefficient of species i . Substituting Eqs. (2), (4) and (5) into Eq. (1) gives the conservation of species i as

$$\rho \frac{\partial f_i}{\partial t} + \rho \vec{v} \cdot \nabla f_i = \nabla \cdot (D_i \nabla f_i) \quad (6)$$

2.2. Conservation of momentum

According to the law of momentum conservation, the rate of change of momentum of fluid within any control volume is equal to the total body and surface forces produced by external means and doing work on the fluid volume. Neglecting external body forces, the momentum conservation equation is given by

$$\rho \frac{d\vec{v}}{dt} = -\nabla \vec{P} + \nabla \cdot \vec{\tau} \quad (7)$$

where \vec{P} is the pressure and $\vec{\tau}$ the stress tensor.

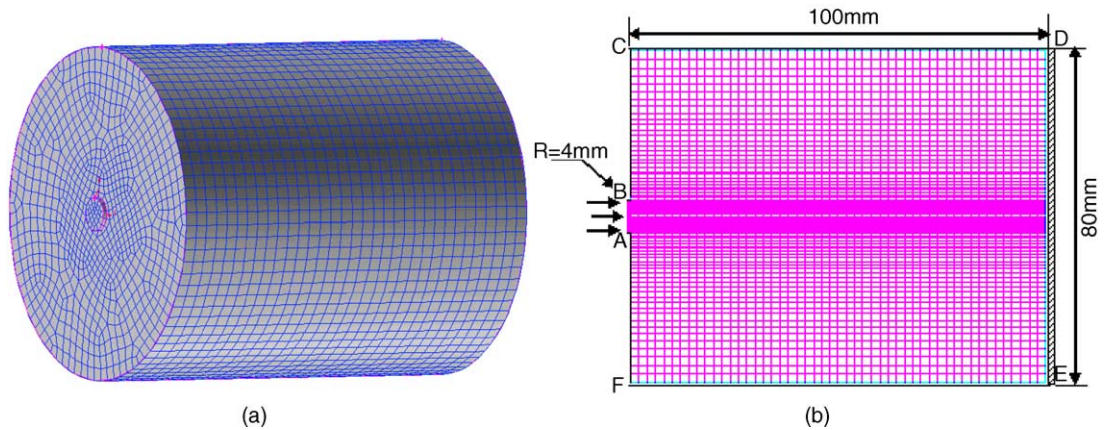


Fig. 1. The geometrical model for the computational domain: (a) 3D model, (b) the vertical section.

2.3. Conservation of energy

Based on the assumptions mentioned above that the energy loss by radiation and chemical reactions are negligible,

the rate of change of fluid enthalpy within a control volume is equal to rate at which the heat is conducted into the fluid, and the rate at which body and surface forces act on the fluid. The conservation of energy can therefore be

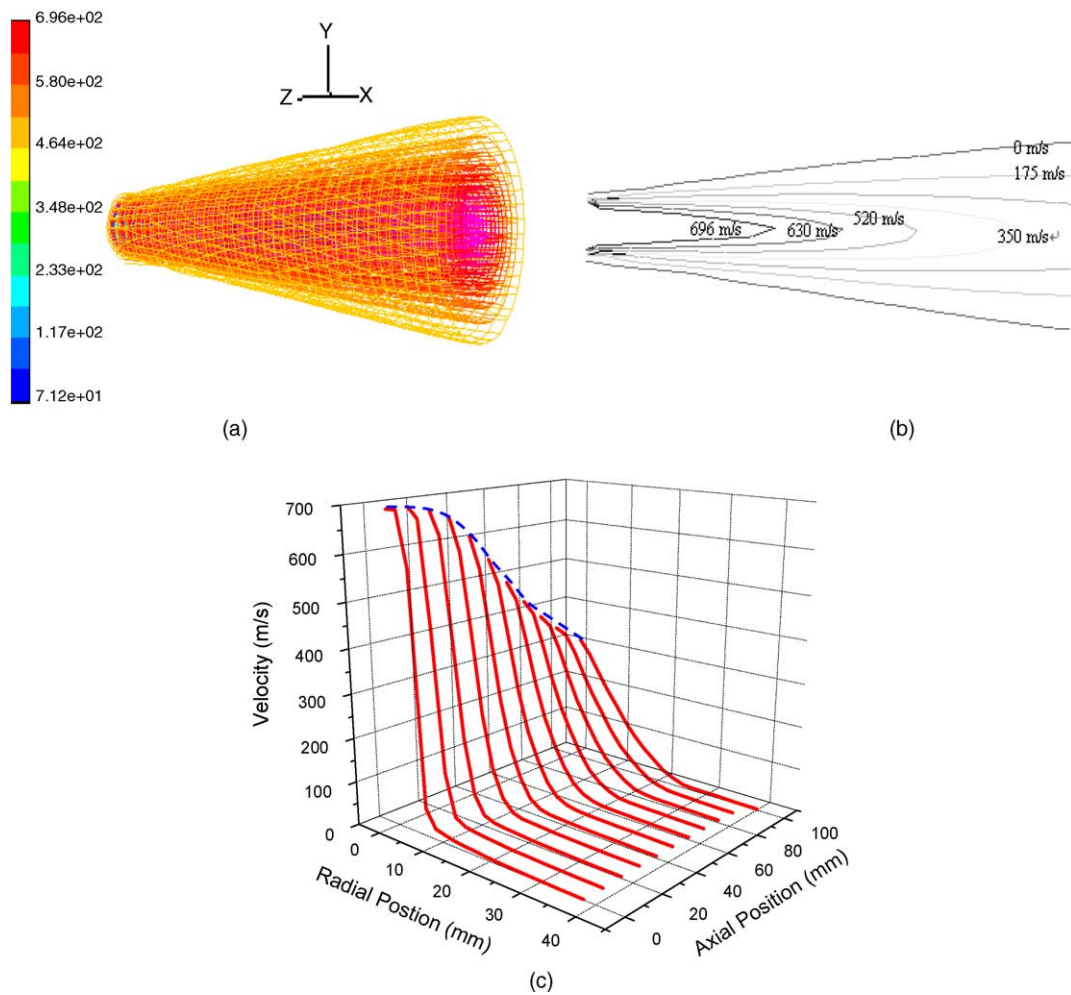


Fig. 2. Velocity distribution in the plasma field: (a) 3D contours of velocity; (b) 2D contours of velocity at the vertical section; (c) 3D velocity continuous distribution along the radial and axial position.

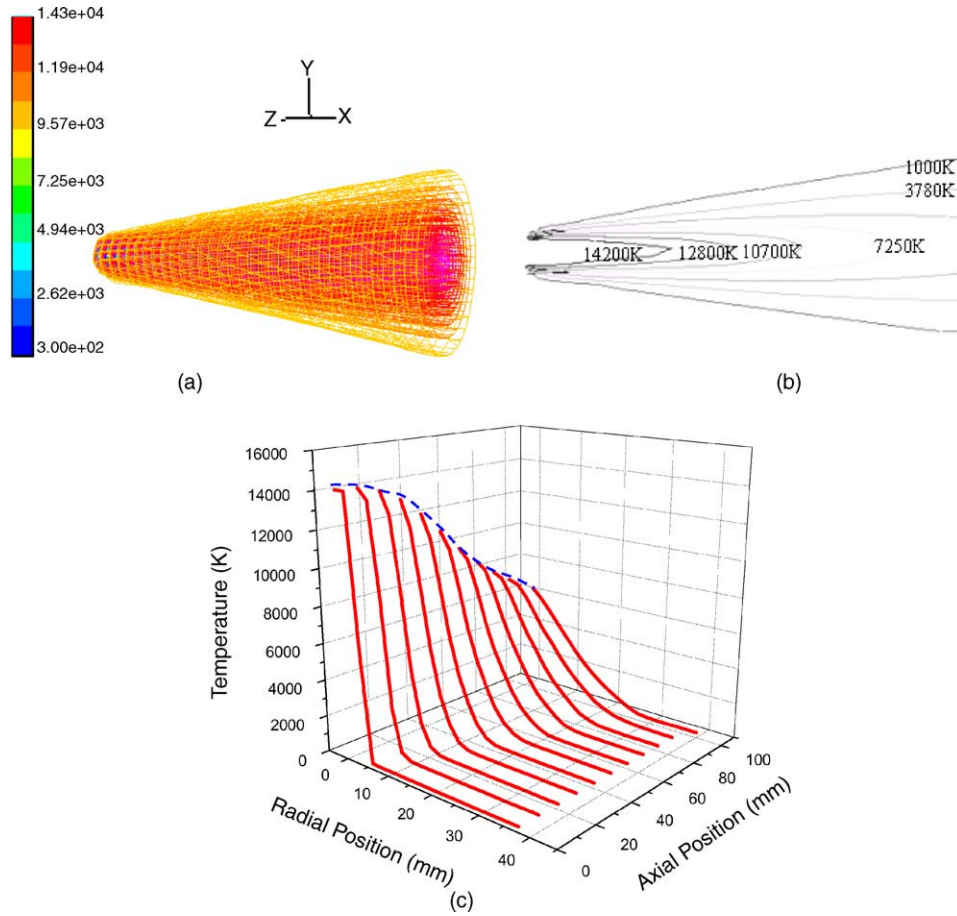


Fig. 3. Temperature distribution in the plasma field: (a) 3D contours of temperature; (b) 2D contours of temperature at the vertical section; (c) 3D temperature continuous distribution along the radial and axial position.

given by

$$\rho \frac{dh}{dt} = -\nabla \cdot \vec{q} - p(\nabla \cdot \vec{v}) + \Phi + \sum_i \rho_i \vec{F}_i \cdot \vec{U}_i \quad (8)$$

where h is the enthalpy; \vec{q} the rate of quantity of heat fluxing into the control volume; Φ the rate of energy loss by viscous friction, which is turned into a thermal form; \vec{F}_i the external body or surface force acting on species i ; and ρ_i the density of species i .

2.4. K - ε equations

As mentioned above the thermal plasma jet is a highly turbulent flow. Modern approaches have formed a strong attachment to the methodology of the discipline of turbulence modeling work of ordinary turbulent flow. However, there are many special features of turbulent thermal plasma which make the modeling work more difficult. For example, many parameters such as the temperature, velocity, concentration and pressure at each point in the plasma field, are functions of temperature.

The K - ε model is the most popular model. It includes two differential equations for the turbulent kinetic energy K and

for its dissipation rate ε . The equations take the following form:

$$\rho \frac{DK}{Dt} = \frac{\partial}{\partial x_j} \left[\left(\mu + \frac{\mu_t}{\sigma_k} \right) \frac{\partial K}{\partial x_j} \right] + G - \rho \varepsilon \quad (9)$$

$$\rho \frac{D\varepsilon}{Dt} = \frac{\partial}{\partial x_j} \left[\left(\mu + \frac{\mu_t}{\sigma_k} \right) \frac{\partial \varepsilon}{\partial x_j} \right] + \frac{\varepsilon}{K} (C_1 G - \rho \varepsilon C_2) \quad (10)$$

where x_j is the velocity component in the direction of j ; μ the viscosity in laminar flow situations; μ_t the turbulent viscosity and can be obtained by $\mu_t = c_\mu \rho k^2 / \varepsilon$; G the dissipation function. C_1 , C_2 , C_μ , σ_k , and σ_ε are constants with the value of 1.44, 1.92, 0.09, 1.0 and 1.3, respectively.

3. Geometry and boundary conditions

The geometrical model shown in Fig. 1(a) is defined as a cylindrical 3D domain, which consists of 26,693 elements. In the radial direction, the grid is more refined near the central axis and coarser towards the outer environment. Fig. 1(b) shows the meshed vertical section and the computational sizes. The plasma jet exit is 8 mm, and the target stands 100 mm away from the jet.

Based on the law of energy balance, the temperature profiles at the torch exit (or the inlet of the free plasma field, see line AB in Fig. 1(b)) can be theoretically derived from the basic processing parameters, including the plasma arc voltage, plasma current, the flow rate of species, etc. Assuming ideal gas behavior, the initial gas velocity at the plasma gun exit can also be given. The two terms are the most basic boundary conditions in the analytical procedure.

In addition, the initial turbulent kinetic energy K_{in} at the nozzle can be calculated by

$$K_{in} = 0.005v_0^2 \quad (11)$$

where v_0 is the initial velocity at the torch exit. The initial dissipation rate ε_{in} may be approximated by the turbulent characteristic length:

$$\varepsilon_{in} = C_\mu \frac{K_{in}^{1.5}}{0.03l_m} \quad (12)$$

where $C_\mu = 0.09$ and l_m is the diameter of the gun exit orifice and regarded as the turbulent characteristic length.

Table 1

The basic plasma spray parameters

Gun nozzle exit (mm)	8
Plasma current (A)	600
Arc voltage (V)	70
Flow rate of Ar (l/h)	2000
Flow rate of H ₂ (l/h)	100
Flow rate of N ₂ (l/h)	100

The temperature, pressure and the mole fractions of species on the other boundaries are specified to be 300 K, the atmospheric pressure and zero, respectively. In addition, the turbulent kinetic energy K and the turbulent dissipation rate ε at the outer boundary of the computational domain are defined as zero.

4. Results and discussion

The basic plasma spray parameters are listed in Table 1.

Fig. 2(a) shows the 3D contours of velocity, which reflects explicitly the 3D appearance of the plasma jet. Fig. 2(b) and

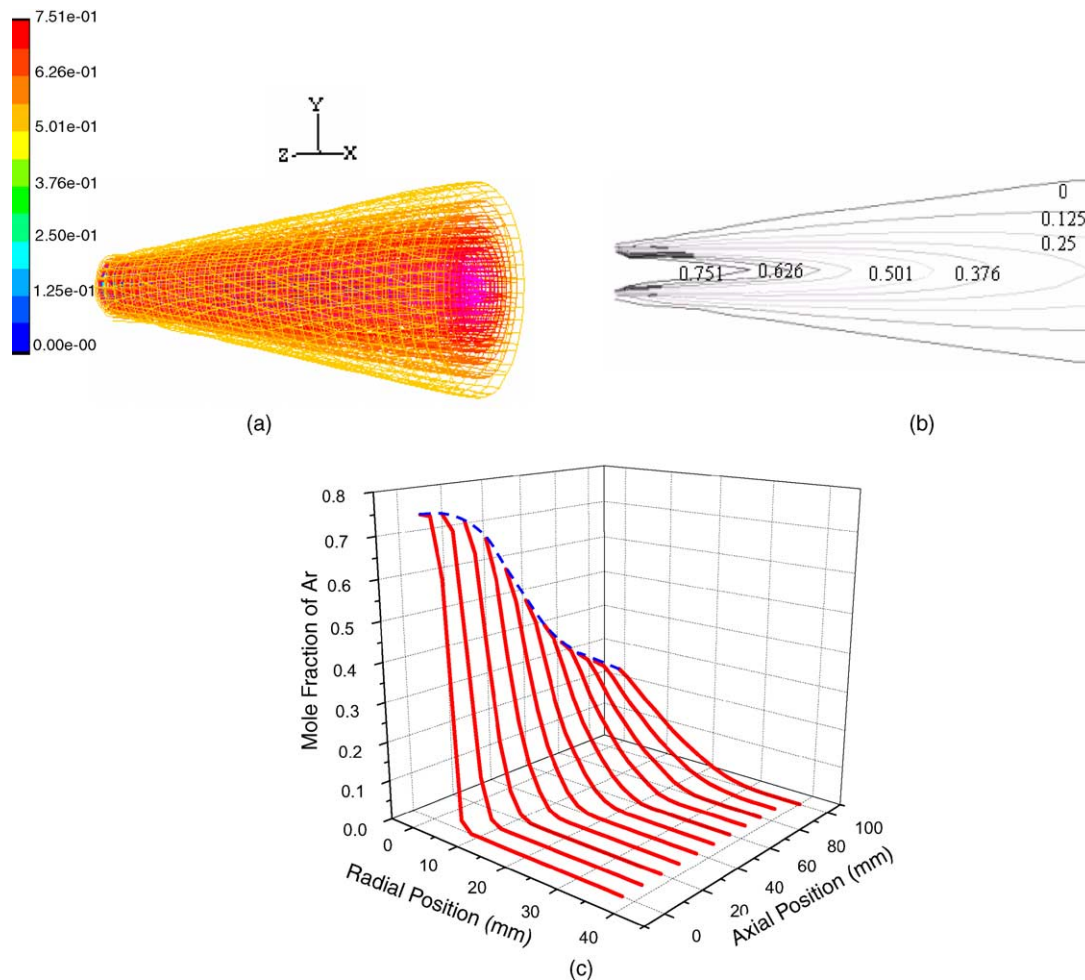


Fig. 4. Distribution of Ar mole fraction in the plasma field: (a) 3D contours of Ar mole fraction; (b) 2D contours of Ar mole fraction at the vertical section; (c) 3D continuous distribution of Ar mole fraction along the radial and axial position.

(c) shows the 2D contours of velocity at the vertical section of the computational domain and the 3D velocity continuous distribution along the radial and axial positions, respectively. It can be seen that, at 100 mm away from the nozzle exit, the corresponding velocity decreases sharply to 300 m/s from the initial 692 m/s. At a certain axial distance, the velocity magnitude along the radial direction also decreases. It might be noted that the decrease rate of the velocity reduces with increasing axial distance. For example, at the axial position of 0 mm, the velocity decreases sharply from 692 to 10 m/s when the radial distance extends outward to 15 mm; however, at the axial position of 100 mm and the radial position of 23 mm, the velocity only decreases to 17 m/s, which is relatively slower. In addition, while the air is entrained into the computational domain, the width of the plasma jet becomes wider with increasing the axial distance as shown in Fig. 2(a) and (b). What is more, the undisturbed zone which keeps the initial velocity dwindles (see Fig. 2(c)) and disappears at some distance.

Fig. 3(a) illustrates the 3D contours of temperature, which also shows the 3D appearance of the plasma jet like Fig. 2(a). Fig. 3(b) and (c) shows the 2D contours of temperature at the vertical section of the computational domain and the 3D temperature continuous distribution along the radial and axial position, respectively. It can be seen that, at 100 mm away from the nozzle exit, the corresponding temperature decreases sharply to 6600 K from the initial 14,200 K. And at a fixed axial distance, the temperature value along the radial direction also decays, as seen in Fig. 2(c). It should be mentioned, however, the decay rate descends with increasing axial distance. For example, at the axial position of 0 mm, the temperature decreases sharply from 14,200 to 300 K when the radial distance extends outward to 8 mm; while at the axial position of 100 mm and the radial position of 25 mm, the temperature falls relatively slower only to 600 K. As the high-temperature jet is injected into the air and expands violently, heat transfer between the two is associated with mass exchange due to the temperature difference. At the outer boundaries, the temperature of the jet decreases and the temperature of the air increases. This means that, the plasma jet is cooled gradually by the ambient air.

Fig. 4(a), 3D contours of Ar mole fraction, closely parallels Figs. 2(a) and 3(a), which reflects the 3D appearance of the plasma jet, too. Fig. 4(b) and (c) respectively shows the 2D contours of argon mole fraction at the vertical section of the computational domain and the 3D continuous distribution of argon mole fraction along the radial and axial position. It can be seen that, at 100 mm away from the nozzle exit, the corresponding Ar concentration decreases sharply to 0 from the initial 0.751. And at a fixed axial distance, the Ar mole fraction along the radial direction also drops, as shown in Fig. 4(c). The decay rate of Ar mole fraction drops as the axial distance increases, like the velocity and temperature fields. For example, at the axial position of 0 mm, the ar-

gon mole fraction decreases sharply to 0, when the radial distance extends outward to 8 mm; at the axial position of 100 mm, however, only when the radial position increases to 30 mm does the Ar concentration approaches 0. Mass transfer is driven by the concentration difference between the plasma and ambient air. Concentration of argon atom and ions in the plasma jet are higher than in the ambient air, so the argon mole fraction in the plasma decreases with increasing axial and radial distances. The mass diffusion mechanism is similar to that in the heat diffusion and presents a tendency from non-equilibrium to equilibrium.

5. Conclusions

In this paper, the plasma velocity, plasma temperature and argon molar concentration distribution in 3D space associated with the 3D appearance of the plasma jet, which are impossible to obtain directly using a 2D scheme, are described by using a continuous medium model and the $k-\varepsilon$ turbulence mathematical representations. As a result it is possible to perform further calculations in future work regarding the residence time and dispersion of multi-group particles in the plasma, the temperature history of the particles, and the temperature history of the deposit formed. Results show that because of high temperature, the plasma expands and flows at a high speed to the ambient air, which results in momentum exchange, heat exchange and mass exchange between the plasma and the air, and hence a sharp decay of velocity, temperature, and Ar mole fraction along the radial and axial directions. In addition, the decay rate is dependent on the axial position under the condition of fixed plasma spray parameters.

References

- [1] E.R.G. Eckert, E. Pfender, *Advances in Plasma Heat Transfer* Advances in Heat Transfer, vol.4, Academic Press, New York, 1967.
- [2] R.N. Szente, R.J. Munz, M.G. Drouet, Cathode erosion in inert gases: the importance of electrode erosion, *Plasma Chem. Plasma Process.* 9 (1) (1989) 121–132.
- [3] N. El-Kaddah, J. Mckelliget, J. Szekely, Heat transfer and fluid flow in plasma spraying, *Metall. Trans. B* 15 (1984) 59–70.
- [4] C.H. Chang, Numerical simulation of alumina spraying in an argon–helium plasma jet, in: *Proceedings of the International Thermal Spray Conference and Exposition*, Orlando, Florida, 1992, pp. 793–798.
- [5] J. Mckelliget, G. Trapaga, E. Gutierrez-Miravete, M. Cybulsky, An integrated mathematical model of the plasma spraying process, in: C. Coddet (Ed.), *Thermal Spray: Meeting the Challenges of the 21st Century*, vol. 1, ASM International, 1998, pp. 335–340.
- [6] B. Dussoubs, P. Fauchais, A. Vardelle, M. Vardelle, Computational analysis of a three-dimensional plasma spray jet, in: C.C. Berndt (Ed.), *Thermal Spray: A United Forum for Scientific and Technological Advances [C]*, ASM International, Materials Park, OH, USA, 1997.
- [7] FLUENT 5.4 User's Guide, Fluent Inc., Lebanon, 1998.